

Generic magnetic field dependence of thermal conductivity in magnetic insulators via hybridization of acoustic phonons and spin-flip excitations

Christopher A. Pocs,¹ Ian A. Leahy,¹ Jie Xing,² Eun Sang Choi,³ Athena S. Sefat,² Michael Hermele,^{1,4} and Minhyea Lee¹

¹*Department of Physics, University of Colorado, Boulder, Colorado 80309, USA*

²*Materials Science and Technology Division, Oak Ridge National Laboratory, Oak Ridge, Tennessee 37831, USA*

³*National High Magnetic Field Laboratory, Tallahassee, Florida, USA*

⁴*Center for Theory of Quantum Matter, University of Colorado, Boulder, Colorado 80309, USA*

(Dated: January 30, 2024)

Magnetic insulators provide excellent playgrounds to realize a range of exciting spin models, some of which predict exotic spin ground states, and thermal transport properties have been taking center stage in probing the spin excitations. Despite the fact that acoustic phonons make the major contribution to heat conduction in a crystalline system, their interplay with magnetic excitations is often viewed as peripheral to the physics of interest, for instance as an inconvenient source of scattering or decoherence. Here, we present a comprehensive study on the longitudinal magneto-thermal transport in a paramagnetic effective spin-1/2 magnetic insulator CsYbSe₂. We introduce a minimal model requiring only Zeeman splitting and magnetoelastic coupling, and use it to argue that hybridized excitations – formed from acoustic phonons and localized spin-flip-excitations across the Zeeman gap of the crystal electric field ground doublet – are responsible for a striking non-monotonic field dependence of longitudinal thermal conductivity. Beyond highlighting a starring role for phonons, our results raise the prospect of universal magneto-thermal transport phenomena in magnetic insulators that originate from simple features shared across many systems.

Thanks to its exclusive sensitivity to itinerant excitations, thermal conductivity is one of the most valuable probes for examining magnetic insulators and for characterizing the magnetic ground state [1–5]. The magnetic field (H) dependence of thermal transport has been argued to be a signature of unconventional spin excitations [6–12]. However, even though phonon excitations of the crystalline lattice are the dominant heat carriers, much of our understanding relies on viewing them in a subsidiary role. When phonons are not entirely neglected in studying the field-dependence of thermal conductivity, one typically considers a thermal current of phonons scattering off spin excitations. While such perspectives can be useful, they can also be oversimplifications that lead us to miss essential physics.

A case in point is the non-monotonic field dependence of thermal conductivity (κ) that has been observed in the paramagnetic states of several effective spin-1/2 magnetic insulators. Namely, (1) $\kappa(H)$ first decreases to a minimum at $H = H_{\min}$ followed by an increase and (2) H_{\min} moves toward large values with increasing temperature. Handful systems have showed this behavior including Cu₃VO₇(OH)₂·H₂O [7], YbTiO₇ [8], Cd-kapellasite [10], gadolinium gallium garnet [13], and α -RuCl₃ above its ordering temperature [14]. Explaining this phenomenology in terms of spin-phonon scattering alone is not plausible, without invoking unusual responses of the spin sector to applied field that seem unlikely to be present across such a wide range of systems. Instead, a generic explanation is called for that involves only common ingredients, and that treats phonon and spin excitations on equal footing.

Here, we propose such an explanation via our study of the well-characterized Kramers pseudospin-1/2 Yb-based triangular lattice CsYbSe₂, where we observed the

non-monotonic field dependence of κ described above. We propose that the longitudinal heat conduction under field is enabled by the hybridized quasiparticles formed from acoustic phonons and spin-flip excitations (SFEs) across the Zeeman gap, and hypothesize that the resulting hybridized excitations are responsible for the non-monotonic $\kappa(H)$. This aligns with a highly simplified theoretical model that qualitatively reproduces key features of the experimental data. The two main ingredients of our model, namely (1) single-ion Zeeman splitting and associated SFEs and (2) magnetoelastic (ME) coupling that mediates phonon-SFE hybridization, are common in magnetic insulators. Therefore, our results offer a starting point to understand the non-monotonic field dependence of κ observed in a range of other systems.

Hybridization is an archetypical manifestation of quantum mechanics, and there is a long history of studying hybridization between phonons and different types of magnetic excitations [15], largely with a focus on spectroscopic properties. More recently, theoretical works [16–20] and one experimental study [21] have considered magnon-phonon hybridization in magnetically ordered systems, and the resulting Berry phase, as a mechanism to generate a (transverse) thermal Hall signal in insulators. In contrast with these prior works, we find dramatic effects of hybridization on the easily measurable longitudinal thermal conductivity. Moreover, while the previous works on thermal Hall effect require particular magnetic orderings or specific forms of spin-spin interaction, our model relies only on ingredients present in *any* effective spin-1/2 system, namely Zeeman splitting and magnetoelastic coupling.

The Yb-based triangular-lattice compound CsYbSe₂ has space group $P6_3/mmc$ and consists of layers of

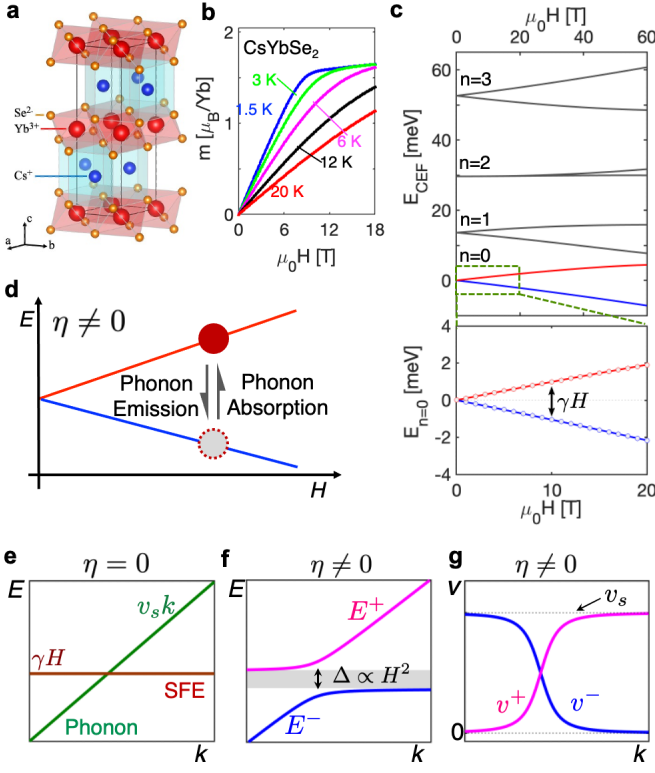


FIG. 1. **a** Crystal structure of CsYbSe₂: Yb³⁺ (red) forms triangular nets within the *ab* plane, formed by edge-sharing YbSe₆ octahedra. **b** Calculated single-ion magnetization within Weiss mean-field approximation [22]. **c** Field dependent crystal electric field energy spectrum calculated with the parameters in [22], where linear splitting of the ground state doublets is shown. The ground state Zeeman gap is γH with $\gamma = 0.22$ meV/T. **d** Schematic illustration of the processes leading to hybridization of phonons and SFEs, where a SFE decays (is created) by emitting (absorbing) a phonon. **e** Schematic sketch of the dispersion relation with no ME coupling ($\eta = 0$). A flat band of SFEs has energy γH , independent of wave vector k , while an acoustic phonon has a linear dispersion with slope v_s . **f** Schematic dispersion relation in the presence of non-zero ME coupling ($\eta \neq 0$), where hybridization leads to an avoided crossing and the opening of a gap between upper and lower branches of hybrid SFE-phonon excitations. **g** Group velocities $v_{\pm} = \frac{dE_{\pm}}{dk}$, derived from the dispersion of the hybridized excitations.

edge-sharing YbSe₆ octahedra separated by Cs³⁺ ions as shown in Fig. 1a [23]. Yb³⁺ carries a $J = 7/2$ magnetic moment, which is split into four doubly degenerate crystal electric field (CEF) levels at zero field. CsYbSe₂ shows no long-range order down to 0.3 K at zero field, with signs of field-induced local correlations below 1 K [24]. Single-ion CEF parameters have been determined in [22], allowing for calculations of the magnetization within the Weiss-mean field approximation [Fig. 1b], which agree well with the magnetization data up to $\mu_0 H = 7$ T. The CEF energy spectrum under field was also obtained and shown in Fig. 1c, where the

Kramers doublets are split via the Zeeman effect under applied field. When the temperature (T) is lowered below the first excitation energy gap ($E_1 - E_0 \simeq 13$ meV), restriction of the dynamics to the ground doublet justifies the use of a pseudospin-1/2 model.

The first order Zeeman splitting of the ground doublet is encoded in the Hamiltonian $\mathcal{H}_Z = \mu_B \mu_0 (g_z H_z \hat{S}^z + g_{\perp} H_x \hat{S}^x + g_{\perp} H_y \hat{S}^y)$, where \hat{S}^i are the pseudospin-1/2 operators and g_z and g_{\perp} the components of the anisotropic g -factor [22]. We always consider field applied along the x -axis (within the crystalline *ab*-plane), so the Zeeman gap of the ground doublet is $\gamma H = g \mu_B \mu_0 H$, where $g \equiv g_{\perp} = 2g_J |\langle 0_{\pm} | \hat{J}_x | 0_{\mp} \rangle|$. Here \hat{J}_x is the angular momentum operator in the direction of the applied field, $|0_{\pm}\rangle$ are the energy eigenstates of the doublet under applied z -axis field, and g_J is the Landé g -factor for the Yb³⁺ ion.

SFEs are excitations across the Zeeman gap, where a single pseudospin is flipped from its $S^x = -1/2$ ground state to the $S^x = +1/2$ excited state. Without hybridization of SFEs and phonons, there is a flat band of non-propagating SFEs (Fig. 1e). Hybridization modifies the dispersion of SFEs and phonons as shown schematically in Fig. 1f, leading to two branches of mixed excitations with non-zero group velocities (Fig. 1g).

The CsYbSe₂ system is particularly well-suited to explore the hybridization of acoustic phonons and SFEs: (1) The CEF gap between the ground and first excited doublets (Δ_{10}) is large enough (~ 13 meV) to provide a large T range where the effective spin-1/2 approximation is valid. (2) The small exchange energy ($J_{\text{ex}} \approx 0.4$ meV) combined with geometric frustration prevents long-range magnetic order [22, 24], leading to a wide paramagnetic regime where spin-spin exchange interactions may be neglected to a first approximation.

Fig. 2 displays the thermal conductivity of CsYbSe₂ as a function of temperature $1.5 \text{ K} < T < 150 \text{ K}$ and field up to $\mu_0 H = 18 \text{ T}$, within the paramagnetic state, where the temperature gradient and field are parallel and within the *ab* plane. For $T < 50 \text{ K}$, the T -dependence of κ is affected by field, where $\mu_0 H = 14 \text{ T}$ enhances (suppresses) κ at low (high) temperatures as shown in Fig. 2a. The non-monotonic field dependence is clarified by plotting κ versus H at several values of T in Fig. 2b. When $T < 5 \text{ K}$, $\kappa(H)$ exhibits weak field-dependence as H is first increased from zero, then rapidly increases upon further increasing H . As T increases above 5 K, $\kappa(H)$ shows a decrease with increasing H until reaching a pronounced minimum at $H = H_{\text{min}}$. The field H_{min} moves to large values as T increases, eventually becoming hard to locate as the field-dependence is diminished. Fig. 2c and d show the fractional thermal conductivity $\Delta\kappa(H)/\kappa_0 \equiv (\kappa(H) - \kappa_0)/\kappa_0$, where κ_0 is the value at zero field at a given T . This quantity is plotted with a constant offset along the y -axis to highlight the monotonic increase of H_{min} with T .

To explain the $\kappa(H)$ data of CsYbSe₂, we need to consider a coupling between phonons and magnetic excita-

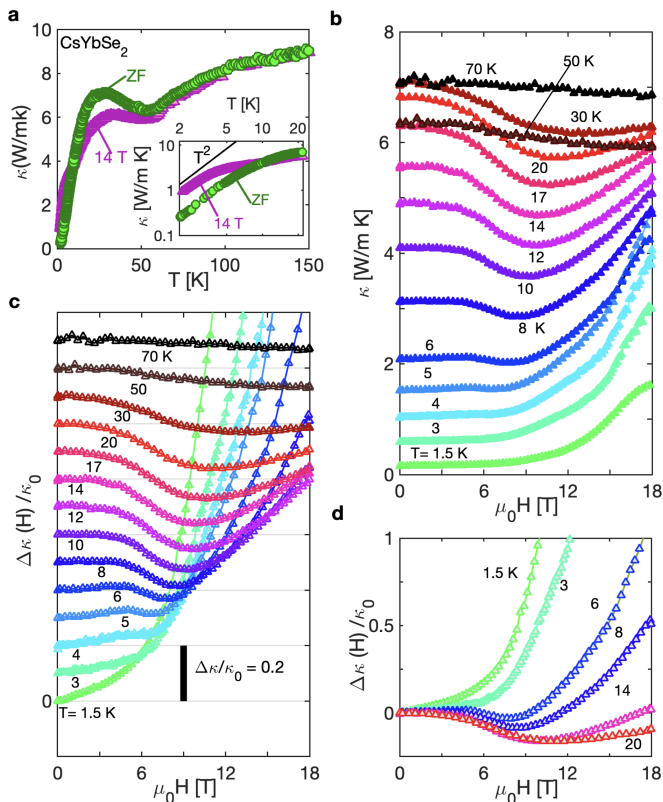


FIG. 2. **a** Temperature dependence of thermal conductivity κ , where $\nabla T \parallel ab$ at zero field and $\mu_0 H = 14$ T, with field aligned to the heat current. Inset shows the magnified view for $T < 20$ K, where T^2 -like behavior can be seen at lower temperatures. **b** Magnetic field dependence of κ is shown at various temperatures. At low temperature $T < 5$ K, $\kappa(H)$ exhibits little field-dependence at small field, followed by a rapid rise as the field is increased through $\mu_0 H \approx 9$ T. Starting above $T = 5$ K, a shallow minimum of $\kappa(H)$ appears at $H = H_{\min}$, where H_{\min} increases with temperature. **c** Fractional thermal conductivity $\Delta\kappa(H)/\kappa_0$, where $\kappa_0 = \kappa(\mu_0 H = 0)$, is plotted as a function of H at various temperatures. The data are plotted with offset for clarity. **d** Fractional thermal conductivity at selected temperatures as indicated.

tions. Recalling that the CEF effect arises from electrostatic interactions between a single magnetic ion and its surrounding ligands, small lattice distortions can create a modulation of the characteristic magnetic energy scales, leading to ME coupling. For example, varying the distortion of YbSe_6 octahedra will change the anisotropy of the g -tensor g_z/g_\perp . At sufficiently low T when only the ground doublet is occupied, the most general linear ME coupling arising from local lattice distortions is $\mathcal{H}_{ME} = \mu_0 \mu_B \sum_{i,j} H_i \delta g_{ij} \hat{S}^j$. That is, ME coupling enters via a modulation of the g -tensor δg_{ij} . For small lattice distortions each component of δg is a linear combination of components of the symmetric strain tensor $\epsilon_{ij} = \partial_i u_j + \partial_j u_i$, where u_i is the displacement field. We note that lattice distortions do not couple to the pseu-

dospin in the limit of zero field, where time reversal symmetry holds and Kramers theorem prevents any splitting of the ground doublet. This contrasts with non-Kramers doublet systems such as TmVO_4 , where the ME coupling remains non-zero in vanishing applied field [25].

The most dramatic consequence of this ME coupling turns out to be the hybridization of SFEs and phonons, arising from terms corresponding to the emission/absorption processes illustrated in Fig. 1c. Here we introduce a highly simplified effective model designed to capture the essential qualitative physics of hybridization as manifested in thermal conductivity. Our model can be motivated by a more microscopic treatment sketched in the Methods Section. The SFEs are treated as bosons within a standard spin wave approximation, and we focus on only a single polarization of acoustic phonon. The energies $E_\pm(k)$ of the two branches of hybridized excitations are the eigenvalues of the matrix

$$\mathcal{H}(k) = \begin{pmatrix} \hbar v_s k & \sqrt{\eta \hbar v_s k} \gamma H \\ \sqrt{\eta \hbar v_s k} \gamma H & \gamma H \end{pmatrix}, \quad (1)$$

where v_s is the sound velocity and $\gamma = g\mu_B\mu_0 = 0.22 \text{ meV}/\text{T}$ as shown in Fig. 1c. From specific heat in zero field (data not shown), we obtained $\hbar v_s = 12.97 \text{ meV \AA}$ equivalent to $2.80 \times 10^3 \text{ m/sec}$ and also the Debye energy $\hbar\omega_D = 7.1 \text{ meV}$. The off-diagonal matrix elements arise from \mathcal{H}_{ME} with ME coupling strength parametrized by η . The \sqrt{k} -dependence matches the scaling of off-diagonal matrix elements within the microscopic treatment illustrated in the Methods Section. Here, we neglect any angular dependence and assume that the hybridized excitations have a spherically symmetric dispersion. The off-diagonal term in Eq. 1 makes it transparent that applied field simultaneously tunes the Zeeman gap γH and the strength of ME coupling.

The energies of hybridized quasiparticles take the form

$$E_\pm(k) = \left(\frac{E_0 + \gamma H}{2} \right) \pm \sqrt{\left(\frac{E_0 - \gamma H}{2} \right)^2 + \eta E_0 \gamma^2 H^2}, \quad (2)$$

where $E_0 = \hbar v_s k$. The dispersion of E_\pm as a function of wavevector k is plotted in Fig. 3a-c for applied fields $\mu_0 H = 4, 8,$ and 16 T, respectively. The Debye energy E_D is marked as a dotted line. The lower branch $E_-(k)$ increases monotonically from zero to $\gamma H - \eta(\gamma H)^2$ as $k \rightarrow \infty$, while the upper branch $E_+(k)$ starts at $E_+(k=0) = \gamma H$ and monotonically increases. The size of the gap (Δ) between the two branches thus takes the simple form $\Delta = \eta(\gamma H)^2$ when including states with arbitrarily large values of k . The gap size increases modestly upon imposing the momentum cutoff $k < \pi/a$ as illustrated by the gray shading in Fig. 3; here, $a = 4.41607 \text{ \AA}$ is the ab -plane lattice constant. Note that the lower branch dispersion becomes flat with $E_-(k) = 0$ when $\eta = (\gamma H)^{-1}$, signaling an instability reached either at large ME coupling or strong applied field, beyond which the model will not be valid. We thus always take $\eta < (\gamma H)^{-1}$, where $E_-(k)$ is non-zero and remains real. Fig. 3d displays a magnified

view in the low-energy region: the slope (*i.e.* group velocity) at $k = 0$ decreases monotonically with increasing field. This is important for determining the high field behavior as discussed below.

Thermal conductivity is computed within a Debye-Callaway model [26] using the above hybridized quasi-particle spectra:

$$\kappa(T, H) = \frac{\tau}{3} \sum_{\sigma=\pm} \int \frac{d\mathbf{k}^3}{(2\pi)^3} c(E_{\sigma}(k)) v_{\sigma}^2(k), \quad (3)$$

$$= \frac{\tau}{3} \int_0^{\infty} dE c(E) v^2(E) g(E). \quad (4)$$

Here, $v_{\pm} = (1/\hbar)dE_{\pm}/dk$ and $c(E) = E dn_B/dT$ is the specific heat of a single bosonic mode, with $n_B(T)$ the standard Bose occupation function. The scattering time τ normally has both temperature and k dependence [26]. However, we always take τ to be k -independent to focus on the effect of hybridization. In Eq. 3, we impose the momentum cutoff $k < \pi/a$. We rewrite κ as an energy integral in Eq. (4), via the density of states $g(E)$ of the hybridized excitations. In Fig. 3e, the integrand of Eq. (4) is plotted for a few values of H at fixed $T = 6$ K. The upper and lower branches are clearly visible as two separate peaks separated by the gap (within which the function vanishes). As the field is increased from zero, the contribution of the upper branch decreases as spectral weight moves to higher energy, while that of the lower branch increases with field.

The measured $\Delta\kappa/\kappa_0$ of CsYbSe₂ and the calculated result are shown Fig. 4a and b, respectively, as a function of applied field. In the calculation, we use $\eta = 0.13$ meV⁻¹, and take τ to be independent of magnetic field, as appropriate for non-magnetic scattering. The temperature dependence of τ plays no role, as it cancels out in the fractional thermal conductivity. Our minimal model qualitatively captures the essential characteristics of the data: non-monotonic field-dependence of κ observed for $T > 5$ K, as well as the movement of H_{\min} to larger values with increasing T . However, there are discrepancies between the data and the model that we return to below.

We now discuss how to understand the non-monotonic field dependence of κ in terms of the hybridized phonon-SFEs based on simple arguments, independent of the details of our model. We assume relatively weak ME coupling such that $\eta\gamma H < c$, where $c < 1$ is an arbitrary dimensionless constant chosen not too close to 1; a simple perturbation theory argument shows that this condition prevents this hybridization from modifying the dispersion too strongly at large wave vector.

First, we consider the low- H regime where $\gamma H \ll k_B T$. In general, excitations contribute more strongly to κ when their energy density changes rapidly with temperature. This is quantified by the heat capacity $c(E)$ of bosonic excitations (inset of Fig. 3e), which appears as a weighting factor in Eq. 4. $c(E)$ is only weakly T -dependent for $E \lesssim k_B T$ and decreases exponentially for $E \gtrsim k_B T$. As in Fig. 3a, upon increasing H , opening

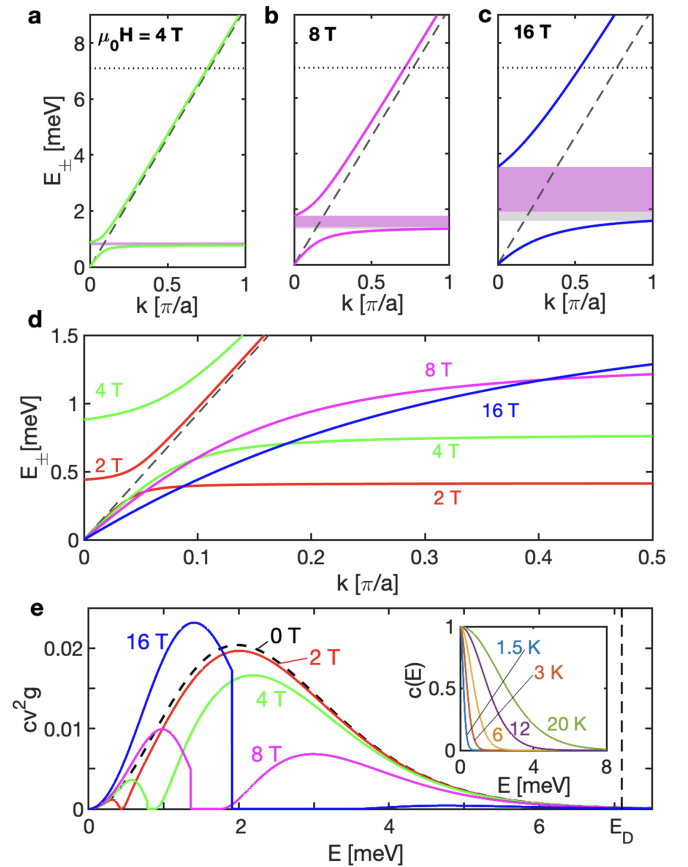


FIG. 3. **a-c** $E_{\pm}(k)$ of Eq.(2) are plotted for $\mu_0 H = 4, 8$ and 16 T, with $\eta = 0.13$ meV⁻¹ and a denoting the lattice constant. The phonon dispersion without ME coupling is shown as a dotted line, while the horizontal dashed line is the Debye energy $E_D = 7.1$ meV. The energy gap (Δ) between upper and low branches, which is proportional to H^2 , is shown with pink and gray shading. The pink shading indicates the gap including states with arbitrarily large values of k , while gray shading shows the increase in the gap upon imposing the cutoff $k < \pi/a$. **d** $E_{\pm}(k)$ for several values of applied field at smaller values of k . The lower branch dispersion near $k = 0$ moves downward in energy (*i.e.* the velocity decreases) with increasing field. **e** The integrand of Eq. (4), $c(E)v^2(E)g(E)$, is shown for several values of applied field at $T = 6$ K. The upper and lower branches are clearly visible as two separate peaks separated by the gap, where $g(E) = 0$. Upon increasing H , the upper-branch contribution decreases as spectral weight moves to higher energy. Meanwhile, the contribution of the lower branch increases with field. The inset plots the specific heat $c(E)$ at selected temperatures.

the gap between upper and low branches pushes spectral weight in the upper (lower) branch to higher (lower) energies. The effect of this on κ is dominated by the upper branch, where $c(E)$ falls off rapidly with energy, and pushing spectral weight to higher energies leads to a decrease in κ , as can be seen in Fig. 3d. On the contrary, for the energy scales in the lower branch, $c(E)$ only depends on weakly on energy and hence the shift in spectral

weight does not strongly affect κ .

Turning to the high-field $\gamma H \gg k_B T$ regime, only lower-branch states with $k \approx 0$ are appreciably thermally occupied, and the lower branch gives the dominant contribution to κ and hence its field-dependence. Moreover, we can approximate the linear dispersion $E_-(k) \approx \hbar v_{\text{eff}} k$ near $k = 0$ (Fig. 3 d). As H increases, level repulsion bends the $k \approx 0$ lower-branch dispersion downward as illustrated in Fig. 3b, resulting in v_{eff} that decreases with increasing field. Within our model, the lower-branch velocity at $k = 0$ is indeed given by $v_- = v_s - v_s \eta \gamma H$. Examining Eq. 4, one might naïvely conclude that κ should decrease as v_{eff} decreases, given the factor of $v(E)^2 \approx v_{\text{eff}}^2$ in the integrand. However, the density of states for a linearly dispersing mode of velocity v_{eff} is $g(E) = E^2 / 2\pi^2 \hbar^3 v_{\text{eff}}^3$, so in fact $\kappa \propto v_{\text{eff}}^{-1}$ in the high-field regime, and κ thus increases with increasing field, which is well-captured in Fig. 4.

Finally, we discuss the discrepancies between the $\Delta\kappa/\kappa_0$ data and the calculation shown in Fig. 4a and b. As compared to the calculation, the data shows a more pronounced increase of $\Delta\kappa/\kappa_0$ at large applied field, and lacks the minimum in $\Delta\kappa/\kappa_0(H)$ for $T < 5$ K. These differences prompt us to consider two simple improvements to our model. First, SFEs are subject to a hard-core repulsive interaction that prevents two excitations from occupying the same lattice site, an effect that becomes more important with increasing temperature due to thermally excited SFEs. In our linear spin-wave treatment of the SFEs, the excitations are represented by bosonic particles that can have arbitrarily high occupation number on a given lattice site. The hard-core repulsive interaction of SFEs can be restored at a mean-field level via temperature-dependent ME coupling $\eta = \eta(T)$, as described in the Methods Section. The coupling $\eta(T)$ is expected to decrease with increasing T due to increased thermal occupation of SFEs. In Fig. 4c, we employ an empirical monotonically decreasing form for $\eta(T)$, as shown in the inset. This correction turns out to have only a small effect on $\Delta\kappa/\kappa_0(H)$ except at the lowest temperatures ($T = 1.5$ K), where it results in a more pronounced increase at large field.

Second, we expect phonons to scatter off of fluctuating paramagnetic moments, with a scattering rate proportional to the effective density of the magnetic scattering centers n_{mag} , which is estimated as $n_{\text{mag}}(T, H) = \frac{\Delta M(T, H)}{M_S} = \frac{M(T, H) - M_S}{M_S}$, where M_S is the saturated magnetization as treated in [27]. Such scattering is thus suppressed with increasing applied field, as the magnetization approaches saturation. This can be incorporated in a simple manner by replacing the scattering rate with $\tau^{-1}(H) = \tau_0^{-1}(1 + \alpha n_{\text{mag}}(H))$ at a given T , where α depends on T and measures the relative strength of magnetic to non-magnetic scattering. Using the field dependence of magnetization calculated in the Weiss mean-field approximation [22] shown in Fig. 1b, we replace the τ in Eq. (3) with $\tau(H)$ above to obtain $\Delta\kappa/\kappa_0$ as a function of H using the same $\eta(T)$ in Fig. 4c and $\alpha(T)$ dis-

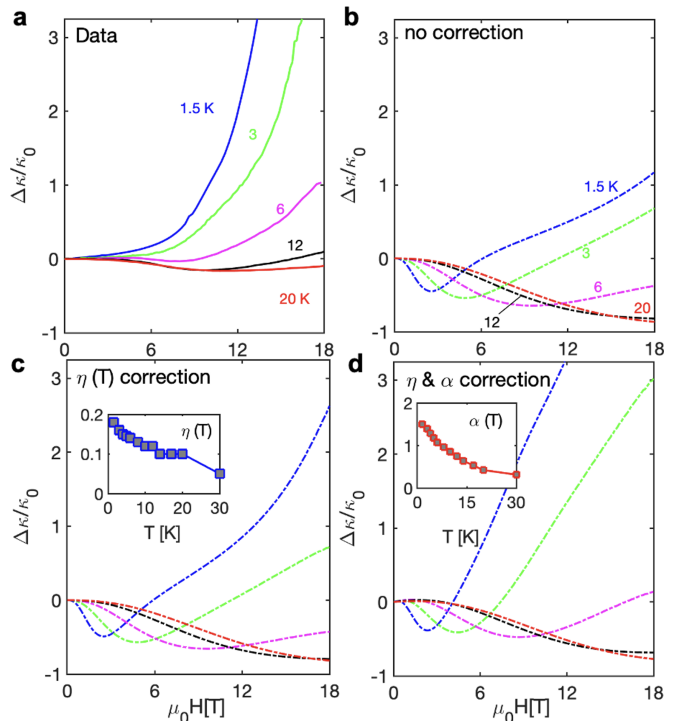


FIG. 4. **a** Comparison of measured and **b** calculated fractional thermal conductivity as a function of applied field at selected temperatures with $\eta = 0.13$ meV $^{-1}$. **c** Calculated $\Delta\kappa(H)/\kappa_0$ including T -dependent ME coupling strength $\eta = \eta(T)$, which incorporates the hard-core nature of SFEs at a mean-field level (see text and Methods). $\eta(T)$ is chosen to optimize qualitative agreement with the data and is shown in the inset. **d** Calculated $\Delta\kappa(H)/\kappa_0$, including scattering of phonons by paramagnetic fluctuations estimated using the deviation from saturation of the magnetization (see text), together with $\eta(T)$ in panel c. The relative strength of magnetic to non-magnetic scattering is quantified by α as described in the text. The temperature-dependence of α (inset) is chosen to optimize qualitative agreement with the data, where the monotonically decreasing $\alpha(T)$ is attributed to non-magnetic phonon-phonon scattering that increases with T .

played in Fig. 4d. We find this correction has a much larger effect: a strong rise in κ at large field and significantly reduced size of the minimum $\Delta\kappa/\kappa_0$ at H_{min} , which further increases the qualitative agreement of the model with the data. However, these corrections do not remove completely the model's pronounced minimum in κ at low T and small applied fields. Needless to say, our minimal model does not account for material-specific details such as spin-spin exchange interactions, proximity to magnetic order, multiple phonon polarizations, and anisotropy in the unperturbed phonon dispersion and ME coupling, all of which may play a role. We also expect that microscopic treatments of scattering processes of the hybridized quasiparticles will bring the model closer to the observed $\Delta\kappa/\kappa_0$.

In summary, our study demonstrated that the field dependence of thermal conductivity in CsYbSe $_2$ can be at-

tributed to heat transport by hybridized quasiparticles formed from acoustic phonons and SFEs. Our highly simplified model qualitatively captures (1) the initial decrease of κ under applied magnetic field to a minimum at $H = H_{\min}$, followed by an increase at higher fields and (2) the monotonic increase of H_{\min} with T . Including an H -dependent relaxation time improves the qualitative agreement between the model and the data. The key ingredients of our model are Zeeman splitting, acoustic phonons, and weak ME coupling via modulation of the magnetic g -tensor by local strain, all of which are found in many systems. We thus expect that phonon-SFE hybridization will be a useful starting point to understand the field dependence of thermal transport in a wide range of magnetic insulators.

ACKNOWLEDGMENTS

We thank Y. Matsuda and Y. Kasahara for helpful discussions. Work at University of Colorado Boulder was supported by the U.S. Department of Energy, Office of Science, Basic Energy Sciences (BES) under Award No. DE-SC0021377 (experimental work by C.A.P., I. A.L. and M.L.) and Award No. DE-SC0014415 (theoretical work by M.H.). Work at Oak Ridge National Laboratory (ORNL) was supported by the U.S. Department of Energy, Office of Science, Basic Energy Sciences, Materials Sciences and Engineering Division. A portion of this work was performed at the National High Magnetic Field Laboratory, which is supported by National Science Foundation Cooperative Agreement No. DMR-1644779, the State of Florida, and the U.S. Department of Energy.

Appendix: Methods

1. Samples and Experimental methods

Millimeter-sized hexagonal shape CsYbSe₂ single crystals were grown by salt flux method following the procedure described in Ref. [23]. The in-plane longitudinal thermal conductivity was measured on the samples of typical dimensions $1.5 \times 3 \times 0.2$ mm³ using a single-heater, two-thermometer configuration in steady-state operation with the field applied in the ab plane and in the direction of the thermal gradient. All thermometry was performed using Cernox resistors, which were precalibrated individually and *in situ* under the maximum applied fields of each instrument.

2. Microscopy Theoretical Treatment

Here we sketch a more microscopic theoretical treatment of the problem of coupled acoustic phonons and

SFEs, which motivates the simplified effective model described in the main text. We treat the acoustic phonons as excitations of a continuous elastic medium with displacement field $u_i(\mathbf{r})$ and symmetric stress tensor $\epsilon_{ij} = \partial_i u_j + \partial_j u_i$. Spin-1/2 spins $\hat{S}_\mathbf{r}^i$ lie on the sites of a Bravais lattice, and the ME coupling takes the form $\mathcal{H}_{ME} = \sum_{\mathbf{r}} \mathcal{H}_{ME}(\mathbf{r})$, where the sum is over lattice sites and $\mathcal{H}_{ME}(\mathbf{r}) = \mu_0 \mu_B H_x \delta g_{xi}(\mathbf{r}) \hat{S}_\mathbf{r}^i$ as described in the main text. (In this Appendix, sums over repeated indices are implied.) We drop the $i = x$ term as it does not lead to hybridization of phonons and SFEs, and the remaining terms can be written $\mathcal{H}_{ME}(\mathbf{r}) = \mu_0 \mu_B H_x [\Lambda_{ij} \epsilon_{ij} \hat{S}_\mathbf{r}^+ + \text{H.c.}]$, where Λ_{ij} is a complex matrix of coupling constants parametrizing the ME coupling and the spin raising operators are defined by $\hat{S}_\mathbf{r}^+ \equiv \hat{S}_\mathbf{r}^y + i \hat{S}_\mathbf{r}^z$ (also $S_\mathbf{r}^- = (S_\mathbf{r}^+)^{\dagger}$ for spin lowering operators). These spin raising/lowering operators are defined to raise/lower $\hat{S}_\mathbf{r}^x$, corresponding to the direction of applied field.

To study the effect of \mathcal{H}_{ME} , we go to momentum space. The Fourier transform of the displacement field is

$$u_i(\mathbf{r}) = \sum_{\mathbf{k}, \lambda} \sqrt{\frac{\hbar}{2V\rho\omega_\lambda(\mathbf{k})}} e^{i\mathbf{k}\cdot\mathbf{r}} \hat{e}_{\lambda i}(\mathbf{k}) [a_{\mathbf{k}\lambda} + a_{\mathbf{k}\lambda}^{\dagger}], \quad (\text{A.1})$$

where V is the volume, ρ the mass density of the crystal, and λ labels the three phonon polarizations with frequencies $\omega_\lambda(\mathbf{k}) = v_\lambda k$, polarization vectors $\hat{e}_\lambda(\mathbf{k})$, and creation operators $a_{\mathbf{k}\lambda}^{\dagger}$. Because we treat the lattice as a continuous medium, the magnitude of the wave vector \mathbf{k} is unrestricted in the sum. For the spin operators, we define the Fourier transform by

$$S_\mathbf{r}^+ = \frac{1}{\sqrt{N}} \sum_{\mathbf{k} \in \text{BZ}} e^{-i\mathbf{k}\cdot\mathbf{r}} S_\mathbf{k}^+, \quad (\text{A.2})$$

where N is the number of lattice sites and the wave vector sum is restricted to the first Brillouin zone.

To make a linear spin-wave approximation, we introduce Holstein-Primakoff bosons with creation operators $b_\mathbf{r}^{\dagger}$ by writing $S_\mathbf{r}^+ = b_\mathbf{r}^{\dagger} \sqrt{1 - b_\mathbf{r}^{\dagger} b_\mathbf{r}}$. We note the form of Eq. (A.2) is chosen so that if we ignore the square root and thus replace $S_\mathbf{r}^+$ by $b_\mathbf{r}^{\dagger}$ and $S_\mathbf{k}^+$ by $b_\mathbf{k}^{\dagger}$, the momentum space creation/annihilation operators satisfy canonical commutation relations. Simply dropping the square root neglects the hard-core nature of the Holstein-Primakoff bosons, but we can restore this effect at a mean-field level by replacing $S_\mathbf{r}^+ \rightarrow \sqrt{1 - \bar{n}} b_\mathbf{r}^{\dagger}$, where $\bar{n} = \langle b_\mathbf{r}^{\dagger} b_\mathbf{r} \rangle$.

Plugging the Fourier transforms into \mathcal{H}_{ME} , keeping only hybridization terms proportional to $a_{\mathbf{k}\lambda}^{\dagger} b_\mathbf{k}$ (or the Hermitian conjugate), and dropping contributions from higher energy phonons outside the first Brillouin zone, we have

- L100402 (2022).
- [20] Bowen Ma, Z. D. Wang, and Gang Chen, “Chiral magneto-phonons with tunable topology in anisotropic quantum magnets,” (2023), arXiv:2309.04064 [cond-mat.mes-hall].
- [21] N. Li, R. R. Neumann, S. K. Guang, Q. Huang, J. Liu, K. Xia, X. Y. Yue, Y. Sun, Y. Y. Wang, Q. J. Li, Y. Jiang, J. Fang, Z. Jiang, X. Zhao, A. Mook, J. Henk, I. Mertig, H. D. Zhou, and X. F. Sun, “Magnon-polaron driven thermal hall effect in a heisenberg-kitaev antiferromagnet,” *Phys. Rev. B* **108**, L140402 (2023).
- [22] Christopher A. Pocs, Peter E. Siegfried, Jie Xing, Athena S. Sefat, Michael Hermele, B. Normand, and Minhyea Lee, “Systematic extraction of crystal electric field effects and quantum magnetic model parameters in triangular rare-earth magnets,” *Phys. Rev. Res.* **3**, 043202 (2021).
- [23] Jie Xing, Liurukara D. Sanjeeva, Jungsoo Kim, G. R. Stewart, Mao-Hua Du, Fernando A. Reboredo, Radu Custelcean, and Athena S. Sefat, “Crystal Synthesis and Frustrated Magnetism in Triangular Lattice CsRESe₂ (RE = La-Lu): Quantum Spin Liquid Candidates CsCeSe₂ and CsYbSe₂,” *ACS Mater. Lett.* **2**, 71 (2020).
- [24] Jie Xing, Liurukara D. Sanjeeva, Jungsoo Kim, G. R. Stewart, Andrey Podlesnyak, and Athena S. Sefat, “Field-induced magnetic transition and spin fluctuations in the quantum spin-liquid candidate CsYbSe₂,” *Phys. Rev. B* **100**, 220407(R) (2019).
- [25] J. K. Kjems, W. Hayes, and S. H. Smith, “Wave-vector dependence of the jahn-teller interactions in tmvo₄,” *Phys. Rev. Lett.* **35**, 1089–1092 (1975).
- [26] R. Bergman, *Thermal conduction in solids* (Oxford University Press, Oxford, 1979).
- [27] Christopher A. Pocs, Ian A. Leahy, Hao Zheng, Gang Cao, Eun-Sang Choi, S.-H. Do, Kwang-Yong Choi, B. Normand, and Minhyea Lee, “Giant thermal magnetoconductivity in crcl₃ and a general model for spin-phonon scattering,” *Phys. Rev. Res.* **2**, 013059 (2020).